Journal of Power Sources 293 (2015) 675–683

Contents lists available at ScienceDirect

Journal of Power Sources

journal homepage: www.elsevier.com/locate/jpowsour

Ceramic separators based on Li^+-conducting inorganic electrolyte for high-performance lithium-ion batteries with enhanced safety

Yun-Chae Jung [a], Seul-Ki Kim [a], Moon-Sung Kim [b], Jeong-Hye Lee [b], Man-Seok Han [b], Duck-Hyun Kim [b], Woo-Cheol Shin [b], Makoto Ue [b], Dong-Won Kim [a, *]

[a] Department of Chemical Engineering, Hanyang University, Seoul 133-791, Republic of Korea
[b] Energy 2 Lab, Battery R&D Center, Samsung SDI, Gyeonggi-do 443-803, Republic of Korea

HIGHLIGHTS

- The flexible ceramic separators based on lithium ion conductor are prepared.
- The ceramic separators show good thermal stability and high ionic conductivity.
- The cells with ceramic separator have good cycling performance and enhanced safety.

ARTICLE INFO

Article history:
Received 20 March 2015
Received in revised form
2 May 2015
Accepted 1 June 2015
Available online 6 June 2015

Keywords:
Ceramic separator
Inorganic electrolyte
Lithium lanthanum zirconium oxide
Lithium-ion battery
Separator-electrode assembly

ABSTRACT

Flexible ceramic separators based on Li^+-conducting lithium lanthanum zirconium oxide are prepared as thin films and directly applied onto negative electrode to produce a separator-electrode assembly with good interfacial adhesion and low interfacial resistances. The ceramic separators show an excellent thermal stability and high ionic conductivity as compared to conventional polypropylene separator. The lithium-ion batteries assembled with graphite negative electrode, Li^+-conducting ceramic separator and $LiCoO_2$ positive electrode exhibit good cycling performance in terms of discharge capacity, capacity retention and rate capability. It is also demonstrated that the use of a ceramic separator can greatly improve safety over cells employing a polypropylene separator, which is highly desirable for lithium-ion batteries with enhanced safety.

1. Introduction

The application of lithium-ion batteries has been expanding from portable electronic devices to large-scale power sources including electric vehicles and energy storage systems, due to their high energy density, high power density and long cycle life [1–7]. Recently, safety issues have become a significant concern for full utilization of these batteries, especially in large-capacity applications. However, organic liquid electrolytes used in present lithium-ion batteries have problems including high flammability, solvent leakage and limited electrochemical stability. In addition, the polyolefin separators that separate the negative and positive electrodes may shrink, soften and even melt at elevated temperatures, which causes a short circuit between the two electrodes in cases where unusually high heat is generated, leading to battery thermal runaway. In this respect, many Li-ion-conducting electrolyte materials have been investigated as alternative electrolytes for lithium-ion batteries to improve battery safety, including solid polymer electrolytes, gel polymer electrolytes, ionic liquid electrolytes and solid inorganic electrolytes [8–14]. Among these, solid inorganic electrolytes present potential advantages, such as an absence of electrolyte leakage, high electrochemical stability, non-flammability, high thermal stability and the absence of problems relating to vaporization of organic solvents. Recently, many studies investigated garnet-type solid ionic conductors as promising Li-ion conducting inorganic electrolytes [15–20]. Among the garnet-structured lithium ion conductors reported so far, the cubic-type lithium lanthanum zirconium oxide (LLZO, $Li_7La_3Zr_2O_{12}$) has been of particular interest, because it exhibits relatively high ionic conductivity, good electrochemical stability (>5.0 V vs. Li/Li^+) and

* Corresponding author.
E-mail address: dongwonkim@hanyang.ac.kr (D.-W. Kim).

http://dx.doi.org/10.1016/j.jpowsour.2015.06.001
0378-7753/

superior chemical stability in contact with lithium metal [16]. However, sheet manufacturing using thin-film technologies for making large-scale lithium-ion batteries is considered very difficult, because ceramic materials are intrinsically hard and brittle. In addition, a lack of flexibility results in poor interfacial contacts between inorganic solid electrolyte and solid electrodes in the cell during charge and discharge cycling [21]. Since the inorganic solid electrolytes are usually prepared as the thick pellet-type, the process compatibility with conventional electrode preparation should be also considered. In order to solve these problems, hybrid solid electrolytes composed of inorganic solid electrolyte and flexible polymer have been investigated, and it was demonstrated that they could synergistically combine the beneficial properties of both ceramics and polymers [22–26]. However, it has been a struggle for these solid-state lithium batteries to obtain competitive cycling performance at ambient temperature, when compared to liquid electrolyte-based lithium-ion batteries. A common problem in the solid-state lithium batteries is their high interfacial resistance between electrolyte and electrodes due to the solid-on-solid interface in the cells. Therefore, it is of great interest to minimize the issues related to solid–solid interfaces, while enhancing battery safety and exhibiting a cycling performance superior to that of lithium-ion batteries employing porous polyolefin separators and organic liquid electrolyte.

In order to achieve this goal, we prepared flexible ceramic separators composed of LLZO as a Li^+-conducting solid electrolyte and poly(vinylidene fluoride-co-hexafluoropropylene) (P(VdF-co-HFP)) random copolymer as a polymer binder. The ceramic separator was directly formed on the negative graphite electrode to produce a separator-electrode assembly (SEA) with good interfacial adhesion and low interfacial resistance. The SEA was employed to assemble lithium-ion batteries composed of a graphite negative electrode and $LiCoO_2$ positive electrode. Our results demonstrate that the lithium-ion batteries assembled with ceramic separators containing Li^+-conducting inorganic electrolyte exhibit superior cycling performance and significantly enhanced safety compared to those of lithium-ion batteries employing conventional polypropylene (PP) separator.

2. Experimental

2.1. Preparation of the ceramic separator

An SEA was prepared by a solution casting method, as schematically illustrated in Fig. 1(a). An appropriate amount of $Li_7La_3Zr_2O_{12}$ (particle size: 1–5 μm, Toshima Manufacturing Co. Ltd.), P(VdF-co-HFP) (Mw = 470,000, Kynar Flex 2801, Arkema) and dibutyl phthalate (DBP, Sigma–Aldrich) were added into the acetone solvent, and the solution was mixed using ball-milling for 12 h. When the complete homogenization of a mixture had occurred, the solution was cast using a doctor blade on the as-prepared graphite negative electrode by allowing evaporation of the solvent. After 1 h, it was immersed in methanol to allow pore formation by DBP removal, and then dried in vacuum oven at 80 °C for 12 h. The contents of LLZO in the ceramic separators were 80 and 90 wt%, and these ceramic separators will be designated as LLZO-80 and LLZO-90, respectively, in this study. The thickness of the ceramic separator in SEA was controlled by adjusting the solid content in the solution. A free-standing ceramic separator was also prepared in order to investigate its characteristics by solution casting on a flat glass plate, as described in the previous case for the preparation of SEA. Despite the high ceramic content, the resulting ceramic separators were obtained in the form of flexible thin film. In order to investigate the effect of ion-conductive LLZO in the ceramic separator, the non-conductive Al_2O_3 particles instead of LLZO particles were also used in preparing the ceramic separator.

2.2. Electrode preparation and battery fabrication

The positive electrode was prepared by coating an n-methyl pyrrolidone (NMP)-based slurry containing $LiCoO_2$, poly(vinylidene fluoride) (PVdF) and super-P carbon (85:7.5:7.5 by weight) onto an aluminum foil. Its active mass loadinga was about 21.2 mg cm^{-2}. The negative electrode was similarly prepared by coating an NMP-based slurry of graphite, PVdF and super-P carbon (88:8:4 by weight) onto a copper foil. The capacity ratio of the negative electrode to the positive electrode was about 1.12. SEA was prepared by applying the solution composed of LLZO and P(VdF-co-HFP) onto the graphite negative electrode, as described above. The lithium-ion battery was assembled via multiple stacking of the positive $LiCoO_2$ electrodes and the SEAs soaked with liquid electrolyte, as schematically depicted in Fig. 1(b). A liquid electrolyte, which consisted of 1.15 M $LiPF_6$ in ethylene carbonate (EC)/diethyl carbonate (DEC) (3:7 by volume, battery grade), was kindly supplied by PANAX ETEC Co. Ltd., and was used without further treatment. The stacked cells were enclosed in a metalized plastic pouch bag and then vacuum-sealed. The nominal capacity of the battery was approximately 670 mAh. For comparison, the lithium-ion battery was also fabricated with a conventional PP separator (Celgard® 2400) and the same liquid electrolyte (1.15 M $LiPF_6$-EC/DEC). All cells were assembled in a dry room.

2.3. Characterization and measurements

A cross section polisher (JEOL IB-09010CP) was used to prepare the cross-section of the SEA. Its cross-sectional morphology was examined using a scanning electron microscope (SEM, JEOL JSM-6300). The elemental distribution on the cross-sectional area of the ceramic separator was examined using energy dispersive X-ray spectroscopy (EDX). X-ray diffraction (XRD) patterns of LLZO and ceramic separators were obtained using an X-ray diffractometer (Rigaku M2500) with Cu Kα radiation. The porosity of the ceramic separators was determined by immersing samples into n-butanol for 1 h and calculated according to Equation (1):

$$\text{Potosity}(\%) = \frac{m_b/\rho_b}{m_b/\rho_b + m_s/\rho_s} \times 100, \quad (1)$$

where m_b is the weight of absorbed n-butanol, m_s is the weight of the separator, ρ_b is the density of n-butanol and ρ_s is the density of the separator [27,28]. To measure the electrolyte uptake and ionic conductivity, the separator was immersed in liquid electrolyte for 1 h, and was taken out from the electrolyte solution; the excess electrolyte solution on its surface was removed by wiping with filter paper. The uptake of the electrolyte solution was then determined by Equation (2):

$$\text{Uptake}(\%) = \frac{W - W_O}{W_O} \times 100, \quad (2)$$

where W_o and W are the weights of the separator before and after soaking in the liquid electrolyte, respectively [29,30]. The separator soaked with liquid electrolyte was sandwiched between two stainless steel electrodes for conductivity measurements. To measure the ionic conductivity, AC impedance measurements were performed using a Zahner Electrik IM6 impedance analyzer over the frequency range of 10 Hz–100 kHz with an amplitude of 10 mV. Charge and discharge cycling tests of the lithium-ion batteries were conducted at a constant current rate over a voltage range of 2.6–4.3 V using battery testing equipment (WBCS 3000,

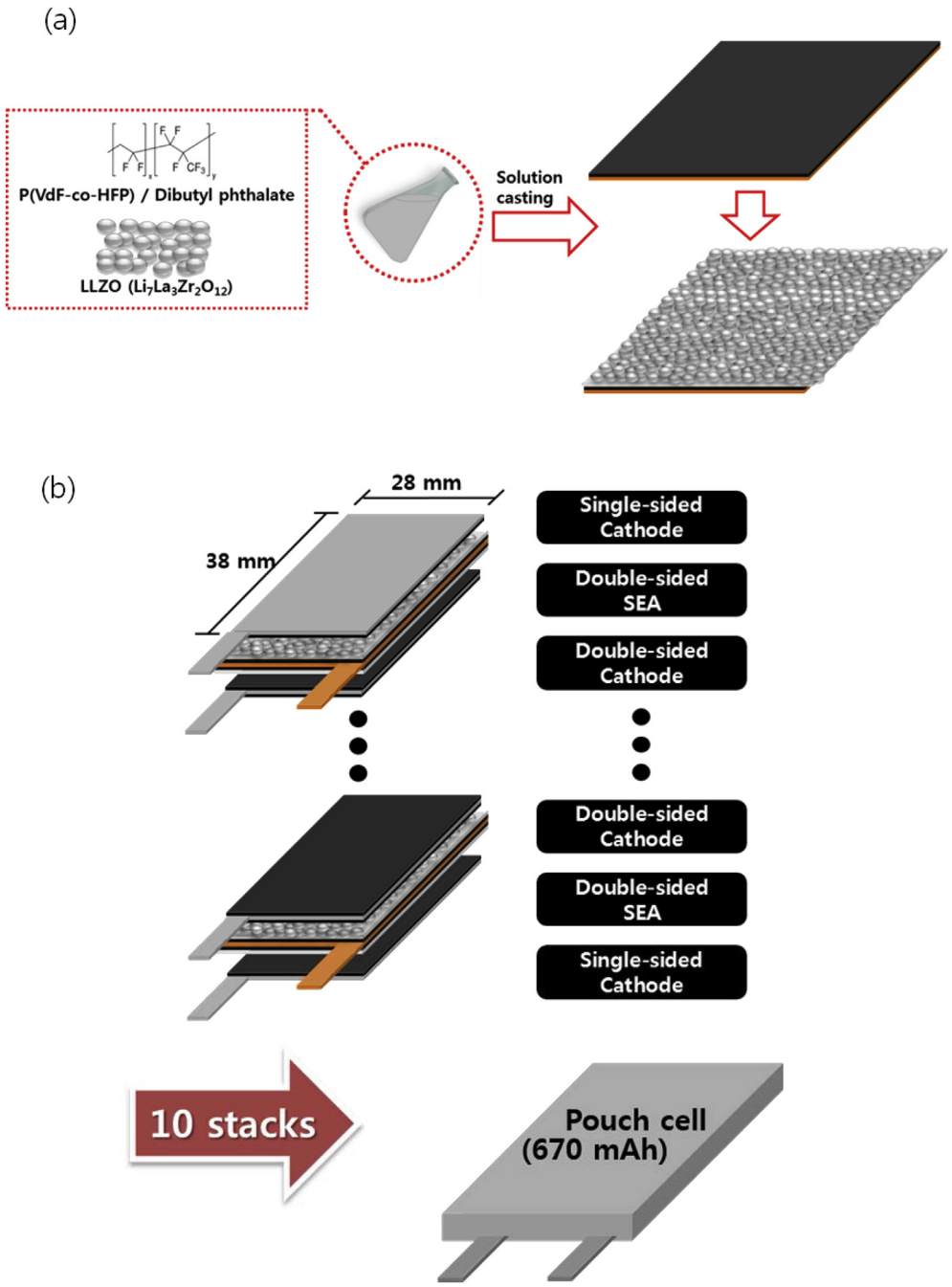

Fig. 1. (a) Schematic representation for preparation of the separator-electrode assembly using lithium lanthanum zirconium oxide and poly(vinylidene fluoride-co-hexafluoropropylene) and (b) fabrication of a pouch-type lithium-ion battery, stacked with separator-electrode (graphite negative electrode) assemblies and $LiCoO_2$ positive electrodes.

Wonatech). Accelerating rate calorimetry (ARC) experiments were performed to analyze the thermal runaway behavior of lithium-ion battery at state of charge (SOC) of 100%. An ARC apparatus (ESARCSYS-001, Thermal Hazard Technology) was operated in a heat, wait, and search mode to allow for determination of the onset of self-heating. It increases the temperature in discrete steps, waits during the thermal transients to decay and then monitors the temperature of the cell for a fixed time period. If the cell temperature does not increase above a threshold value (0.02 °C min^{-1}), the temperature is increased by another step and the process repeats. If the cell temperature increases at rate above 0.02 °C min^{-1}, it switches to the exothermic mode during which the ARC temperature closely matches the cell temperature, thus maintaining the adiabatic state. A nail penetration test was performed to investigate the thermal behavior of lithium-ion pouch cells under abuse conditions. The test was carried out on pouch cells at SOC 100%, placed on an iron plate in a closed chamber using a nail (90 mm long, 2.5 mm diameter) which penetrated the center of the cell at a rate of 10 mm s^{-1}.

3. Results and discussion

Fig. 2(a) shows the SEM image of the cross-sectional area for SEA prepared with LLZO-80 and an enlarged cross-sectional image of the ceramic separator is shown in Fig. 2(b). The thickness of the ceramic separator formed on the negative electrode was about

32 μm. LLZO powders were found to be homogeneously distributed and well embedded in the ceramic separator, indicating that the content of polymer was appropriate for effectively binding the ceramic particles without agglomeration. The ceramic separator exhibited a submicron pore structure, which enabled absorption of liquid electrolyte into the porous ceramic separator. The SEA was not physically separated into the ceramic separator and the negative electrode. Different from the conventional polyolefin separators, the ceramic separator was directly applied onto the negative electrode via solution casting, which could enhance the interfacial adhesion between the ceramic separator and the negative electrode. Fig. 2(c)–(f) present the EDX mapping images of various elements (La, Zr, O and F) on the cross-section of SEA shown in Fig. 2(a). It is evident that La, Zr and O elements arising from the LLZO particles are evenly distributed across the image. The fluorine elements from P(VdF-co-HFP) and PVdF are also uniformly dispersed in the ceramic separator and graphite negative electrode, respectively. It should be noted that some of La, Zr and O elements could be also found in the negative electrode layer. This result suggests that some of the LLZO particles penetrated into the pores of the negative electrode during the casting process of ceramic solution onto the electrode, resulting in good interfacial contacts between the ceramic separator and negative electrode. Good adhesion to the negative electrode can decrease the interfacial resistances and reduce the lithium dendrite formation on the negative electrode upon overcharge [31,32].

Fig. 3 shows the XRD patterns of pristine LLZO powder and ceramic separators of various compositions (LLZO-80 and LLZO-90). The measured XRD pattern of LLZO powder matched the standard pattern of the known garnet phase $Li_5La_3Nb_2O_{12}$ (JCPDS 80-0457), as shown in figure [17]. The lattice parameter for the cubic-type crystalline LLZO phase was determined to be $a = 12.9580 \pm 0.0045$ Å from the least-squares method. The crystalline peaks of LLZO powder in the ceramic separators with

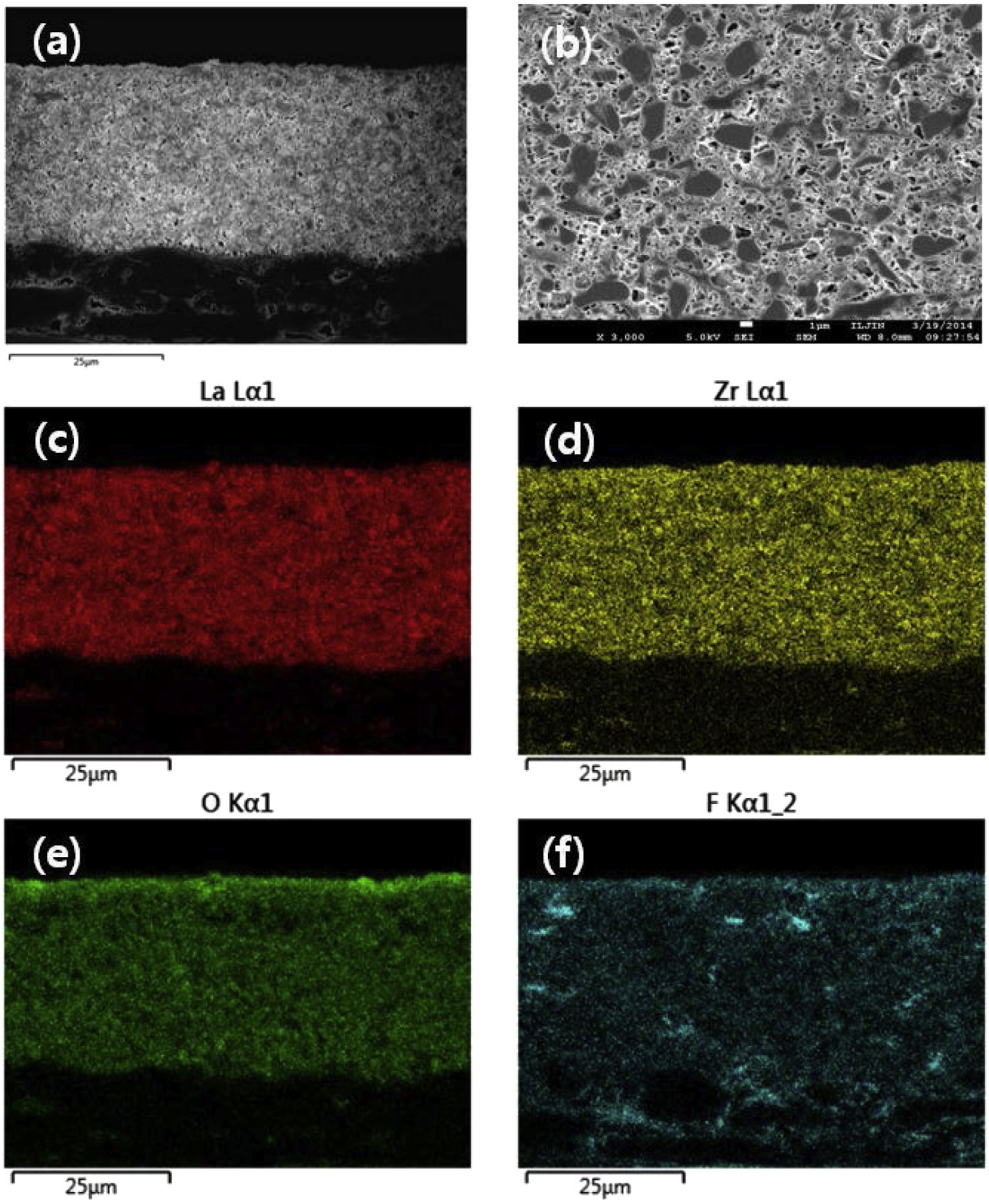

Fig. 2. (a) Cross-sectional SEM image of separator-electrode assembly prepared with LLZO-80, (b) an enlarged cross-sectional SEM image of ceramic separator, and EDX mapping images of (c) La, (d) Zr, (e) O, and (f) F on its cross-section.

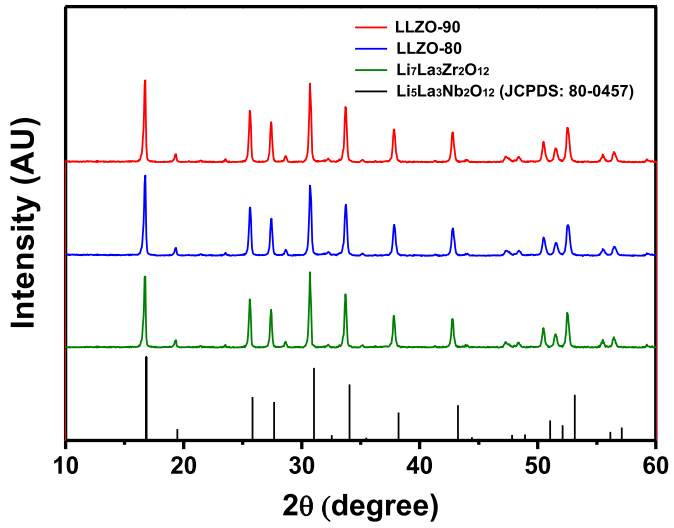

Fig. 3. XRD patterns of pristine LLZO powder and ceramic separators (LLZO-80 and LLZO-90).

compositions of LLZO-80 and LLZO-90 were almost the same, without any broadening or shifting, when compared to those of pristine LLZO powder. This result supports that there are no reactions or degradations between LLZO and P(VdF-co-HFP) in the ceramic separator.

To evaluate the heat resistance of PP and ceramic separators, we investigated their thermal shrinking behavior after storing them at 150 °C for 60 min; the results are compared in Fig. 4. As clearly shown in this figure, the PP separator exhibited a high degree of shrinkage after the high-temperature exposure. When the temperature rises to the softening temperature, the PP separator tends to shrink, even if the porosity is very low, because of the difference in the density between the crystalline and amorphous phases of polyolefin materials [33,34]. The manufacturing process of PP separators includes a drawing step to enlarge porosity, and thus the separator also easily shrinks when exposed to high temperature. Since the thermal shrinkage may cause short circuits between electrodes, it should be minimized. It should be noted that the thermal shrinkage did not occur in the ceramic separators (LLZO-80 and LLZO-90). The presence of heat-resistant LLZO particles with small amounts of polymer binder in the ceramic separator was considered as an effective way to prevent dimensional changes via thermal deformation at high temperatures.

The porosity, electrolyte uptake, and ionic conductivity of various separators soaked with liquid electrolyte are given in Table 1. The porosities of the ceramic separators were 38.3 and 39.8% for LLZO-80 and LLZO-90, respectively, which were slightly lower than that of the PP separator. The uptake of electrolyte solution in ceramic separators was lower than that of the PP separator, due to their lower porosity and higher skeletal density. Ionic conductivity of the PP separator filled with the electrolyte solution was 4.5×10^{-4} S cm^{-1}, which was much lower than that of the electrolyte solution (7.0×10^{-3} S cm^{-1}). It is well known that the ionic conductivity of separators saturated with liquid electrolyte is lowered due to the combined effects of the separator's tortuosity and porosity. The MacMullin number (N_M), the ratio of the ionic conductivity of the pure liquid electrolyte (σ_0) to that of the separator filled with liquid electrolyte (σ_{eff}), is used to characterize this behavior by the following equation: $N_M = (\sigma_0/\sigma_{eff}) = (\tau^2/\varepsilon)$, where τ is the tortuosity and ε is the porosity of the separator [33,34]. According to a previous report, the MacMullin number of the PP separator (Celgard 2400) is approximately 16 ± 2 [35], which means that use of the PP separator sharply decreases the ionic conductivity in the cell. It should be noted that the ionic conductivities were higher in the ceramic separators than that measured in the PP separator, even though their porosity and uptakes were lower. This result suggests that the lithium ion conduction in LLZO contributes to the ionic conductivity in the ceramic separator. In addition, the capability of P(VdF-co-HFP) to form a gel polymer electrolyte can also contribute to the high ionic conductivity; accordingly, the lithium ions can migrate with less tortuous ionic paths between two electrodes. In order to investigate the contribution of LLZO particles to ionic conductivity in the ceramic separator, we compared the ionic conductivities of ceramic separators prepared with 80 wt% LLZO particles (LLZO-80) and 80 wt% Al_2O_3 particles (Alumina-80), respectively. As a result, the LLZO-80 separator soaked with liquid electrolyte exhibited higher ionic conductivity (1.1×10^{-3} S cm^{-1}) as compared to the Alumina-80 separator containing same content of liquid electrolyte (7.4×10^{-4} S cm^{-1}). Since the Al_2O_3 particles are insulators, they may block the Li ion transport in the ceramic separator. In contrast, LLZO is a single ion conductor that transports only Li^+ ions, and thus the higher ionic conductivity in LLZO-80 indicates that the LLZO particles in the ceramic separator contribute to the ionic conductivity. Accordingly, the higher ionic conductivity when employing LLZO particles arises from a combination of solid and gel polymer electrolyte and not from the liquid electrolyte alone, as previously reported in inorganic solid/organic liquid hybrid electrolytes [21].

The cycling performance of lithium-ion pouch cells assembled with ceramic separators was evaluated. The assembled cells were initially subjected to a preconditioning cycle over a voltage range of 2.6–4.3 V at a constant current of 67 mA (0.1C rate). After two cycles at the 0.1C rate, the cells were charged at 335 mA (0.5C) up to a set voltage of 4.3 V, followed by a constant voltage charge until the final current reached 10% of the charging current. The cells were then discharged down to a cut-off voltage of 2.6 V at the same current (335 mA, 0.5C). Fig. 5(a) shows the typical charge and discharge curves of the lithium-ion pouch cell assembled with a ceramic separator (LLZO-80). The cell initially delivered a discharge capacity of 669.4 mAh, which corresponded to a specific capacity of 148.8 mAh g^{-1} based on the active $LiCoO_2$ material in the positive electrode. The discharge capacity decreased to 618.1 mAh at the 300th cycle, corresponding to 92.3% of the initial value. The coulombic efficiency steadily increased with the cycle number, and was maintained at >99.8% throughout cycling after stabilizing. Fig. 5(b) shows the discharge capacities as a function of the cycle number in the cells assembled with a PP separator and ceramic separators. The cycling stability is clearly better in the cells with the ceramic separator. The compact interfacial contact between the ceramic separator and the electrodes can contribute to the good cycling stability. Use of less liquid electrolyte in the ceramic separator may also prevent exudation of the electrolyte solution, as well as suppressing harmful interfacial side reactions between the electrodes and the electrolyte, which results in good cycling stability. Fig. 5(c) shows the AC impedance spectra of cells with different separators, which are obtained at the charged state after 300 cycles. All of the spectra exhibited two overlapping semicircles, which were assigned to the resistance of Li^+ ions through the SEI film at the electrode surface and the charge transfer resistance at the electrode–electrolyte interface [36,37]. The electrolyte resistance corresponding to the high-frequency intercept at the real axis was higher in the cell with a PP separator, as shown in the inset of Fig. 5(c). This result can be ascribed to lower ionic conductivity in the PP separator, loss of electrolyte solution due to leakage and deleterious reactions between the electrolyte and the electrodes during cycling. It was also found that the cells with ceramic

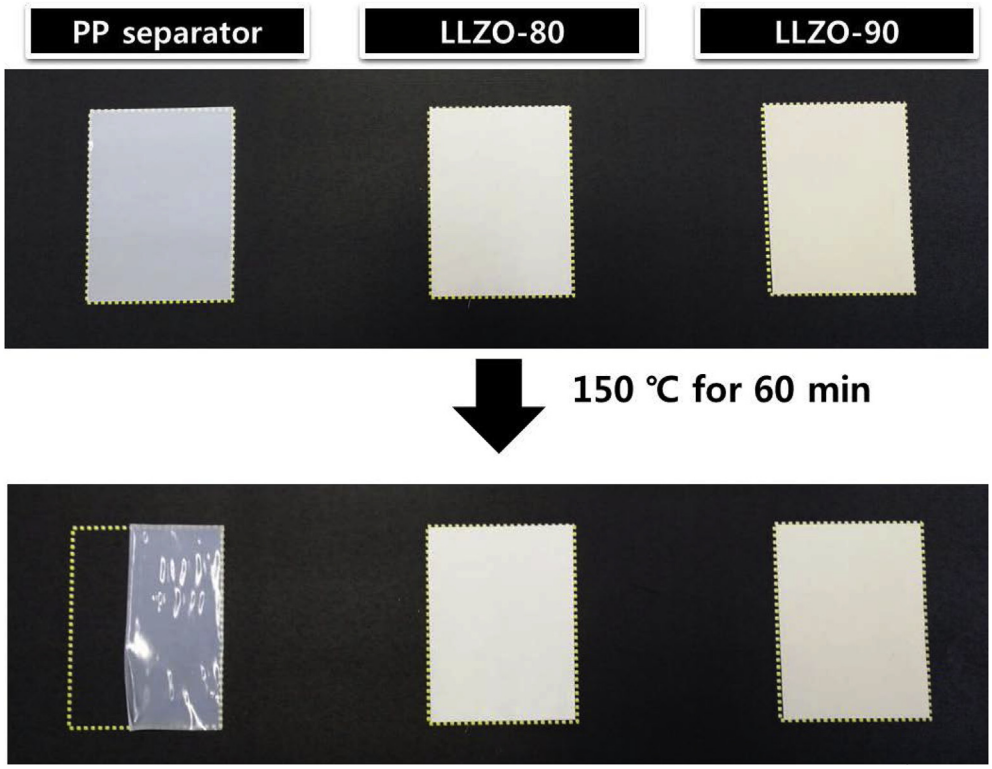

Fig. 4. Photographs of various separators before and after 150 °C exposure for 60 min.

Table 1
Physical properties, electrolyte uptake and ionic conductivities of PP and ceramic separators soaked with liquid electrolyte.

Separator	Thickness (μm)	Porosity (%)	Electrolyte uptake[a] (%)	Ionic conductivity (S cm^{-1})
PP	25	41.0	80.3	4.5×10^{-4}
LLZO-80	30	38.3	23.2	1.1×10^{-3}
LLZO-90	30	39.8	23.5	1.3×10^{-3}

[a] The soaking electrolyte was 1.15 M $LiPF_6$-EC/DEC.

separators had lower interfacial resistances than the cells with a PP separator. This result implies that the cells with ceramic separators have more stable electrode–electrolyte interfaces, resulting in good capacity retention.

Fig. 6 shows comparisons of the discharge capacities of lithium-ion batteries assembled with various separators during experiments in which the C rate was increased every five cycles within the range of 0.1–2.0C. Discharge capacities decreased as the C rate increased, which reflects the polarization. It can be seen that the discharge capacities of the cells with ceramic separators were higher than those of cells with a PP separator for all C rates tested. This superior rate capability can be ascribed not only to the higher ion conductivity in the ceramic separators, but also to lower interfacial resistance due to better interfacial contacts between the ceramic separator and electrodes in the lithium-ion cell assembled with SEA. The batteries with ceramic separators recovered 99.8% of the initial discharge capacity at a rate of 0.1C after high current rate cycles, indicating good cycling stability.

Fig. 7(a) shows the self-heating rate as a function of temperature in the lithium-ion batteries assembled with a PP separator and LLZO-80. The heating rates are only shown for the exothermic regions where the self-heating rate exceeded 0.02 °C min^{-1}. The cell employing the PP separator exhibited a thermal trigger for self-heating near 60 °C and a thermal ignition with continuous self-heating after 455 min. On the other hand, the cell with the ceramic separator showed a thermal trigger for self-heating around 80 °C and ignited after 1107 min, which was much later than the cell with the PP separator. Fig. 7(b) shows the difference in the self-heating rate as a function of temperature in the cells with a PP separator and LLZO-80. The data on self-heating rate seem to be noisy up to 60 and 80 °C for PP separator and LLZO-80, respectively. Since the cell temperature did not increase at rate higher than 0.02 °C min^{-1} in this region, the temperature was externally increased by ARC apparatus at rate of 10 °C min^{-1} until the self heating rate of the cell was higher than 0.02 °C min^{-1}. This is a reason why the data are noisy in the beginning of ARC test. With increasing temperature, the self-heating rate of the cell with LLZO-80 was approximately 3 times lower than that of the cell with the PP separator up to 153 °C. According to previous reports [38–40], the thermal decomposition of solid electrolyte interphase (SEI) layer occurs near 130 °C. It should be noted that the amount of heat generated around 130 °C was significantly reduced in the cell with the ceramic separator, as shown in Fig. 7(b). This result implies that the ceramic separator directly formed on the negative electrode protects the thermal decomposition of the SEI layer and lowers the self-heating rate by reducing the reactivity between the electrolyte solution and the negative electrode, because s stable SEI layer can be formed due to the intimate contacts between the ceramic

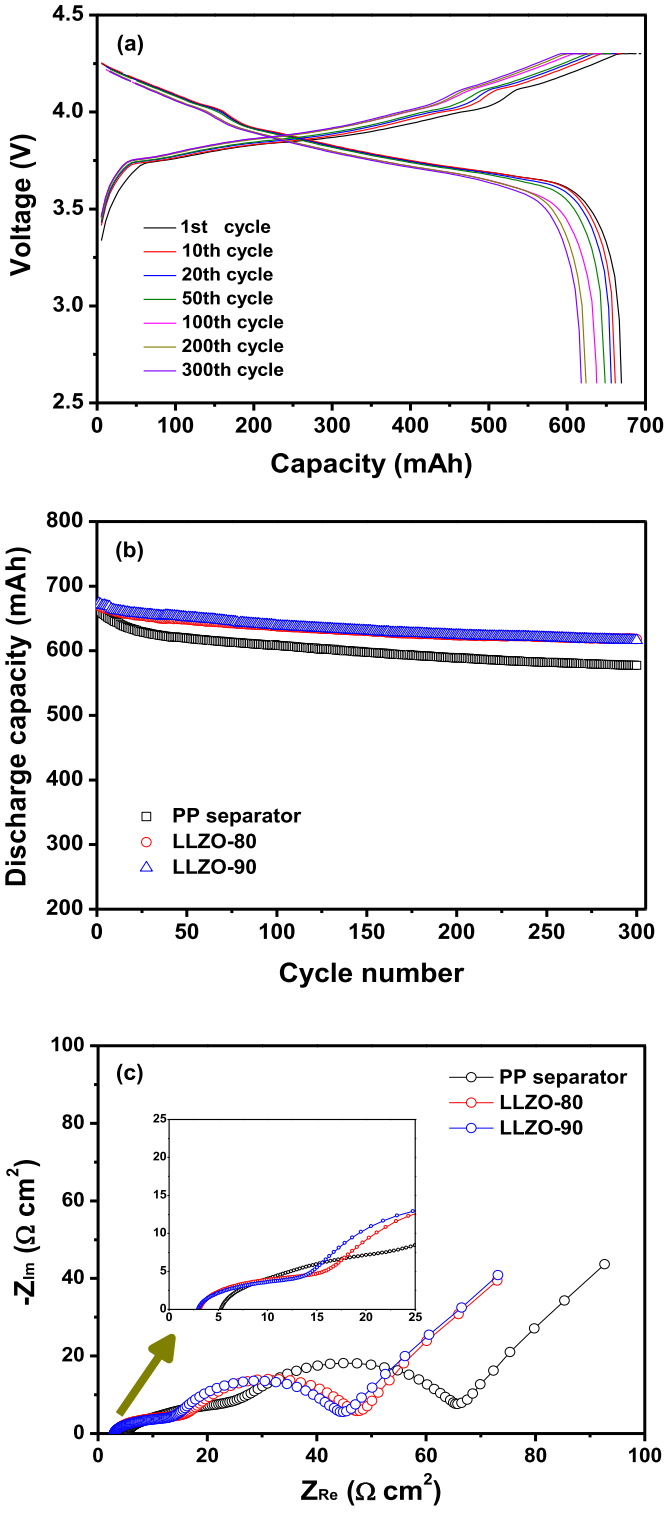

Fig. 5. (a) Charge and discharge curves of the lithium-ion battery assembled with a ceramic separator (LLZO-80) at 25 °C (0.5C CC and CV charge, 0.5C CC discharge, cut-off: 2.6–4.3 V), (b) discharge capacities of the lithium-ion batteries assembled with various separators, and (c) AC impedance spectra of the lithium-ion batteries after 300 cycles.

separator and the negative electrode, as depicted in Fig. 2. Moreover, cell ignition due to the thermal shrinkage and combustion of the polymeric separator can be remarkably suppressed by replacing a PP separator with a ceramic separator. The cell explosion near

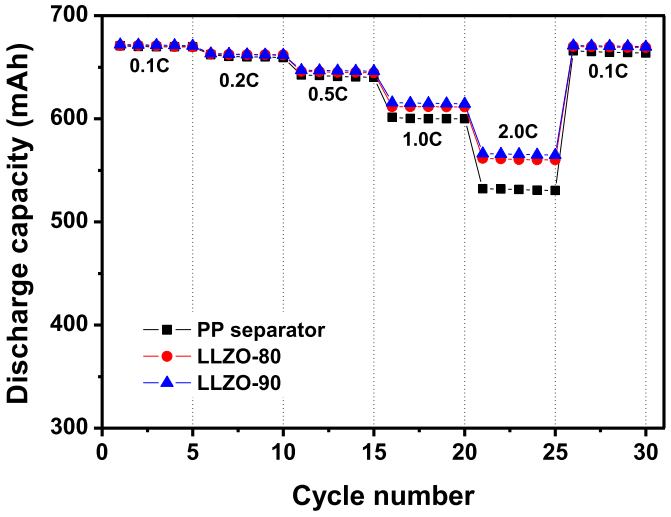

Fig. 6. Discharge capacities of the lithium-ion batteries assembled with various separators as a function of C rate.

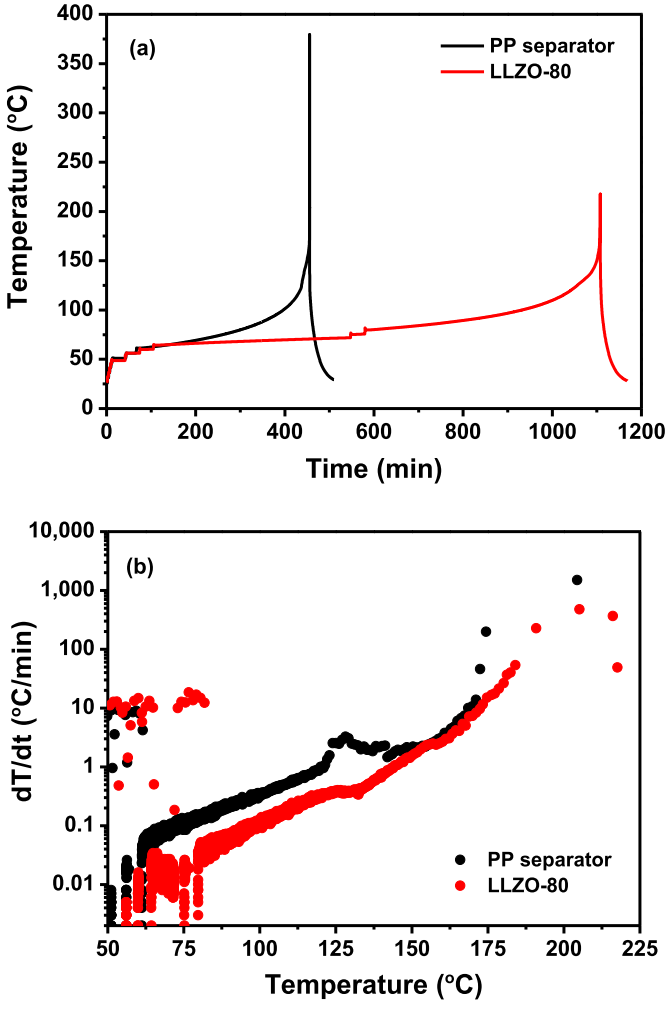

Fig. 7. Self-heating rate as a function of temperature in the stack cell assembled with PP (black) and ceramic separator (LLZO-80) (red). (a) Time vs. temperature and (b) temperature vs. dT/dt. (For interpretation of the references to color in this figure legend, the reader is referred to the web version of this article.)

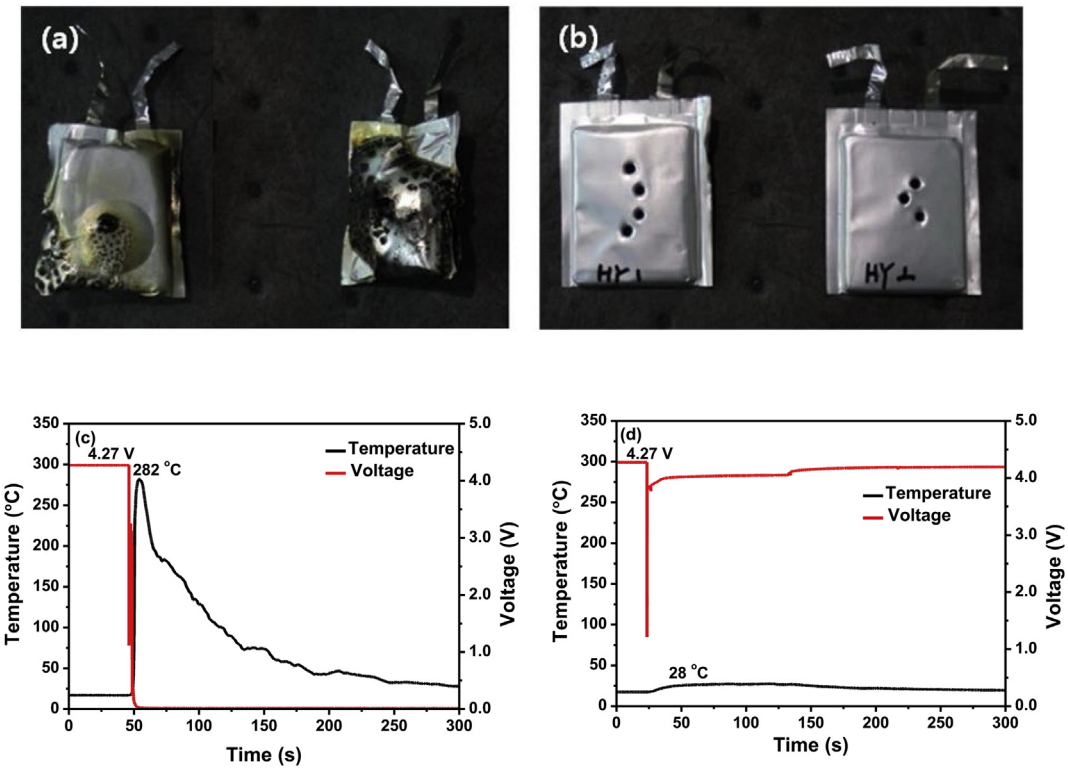

Fig. 8. Photographs of pouch cells assembled with (a) PP and (b) ceramic separator (LLZO-80) after a nail penetration test, and cell voltage and temperature profile of pouch cells assembled with (c) PP and (d) ceramic separator (LLZO-80) during the nail penetration test.

170 °C was accompanied by an increase in the rate of heat generation in the cell. The cell assembled with a PP separator showed an accelerated self-heating after explosion, while the cell with the ceramic separator exhibited a significantly lower self-heating rate in this temperature region. These results suggest that the use of a ceramic separator can enhance battery safety by suppressing the thermal runaway in the event of overheating.

Lithium-ion batteries were subjected to nail penetration, and photographs of the pouch cells taken after the test are presented in Fig. 8(a) and (b). The pouch cell assembled with a PP separator expanded as gasses built within, and eventually ruptured. In contrast, the pouch cell with the ceramic separator maintained its original shape without expansion or rupture. Fig. 8(c) and (d) show the cell voltage and cell surface temperature during the nail penetration test. It is worth noting that the two cells showed quite different voltage and thermal responses upon nail penetration. Both cells showed a constant voltage and temperature before the tests were conducted. In the pouch cell assembled with a PP separator, the cell voltage fell to zero and the cell temperature abruptly increased to 282 °C at the instant the experiment started, which can be attributed to a high surge of current resulting in massive heat generation followed by PP separator meltdown and contact between the negative and positive electrodes. In contrast, the pouch cell assembled with a ceramic separator did not exhibit a significant temperature increase. The cell voltage instantaneously fell to 1.21 V and recovered to 3.84 V within 1.0 s. In this cell, LLZO particles in the ceramic separator allowed it to maintain original dimensions without direct contact between negative and positive electrodes. At the same time, the gel polymer formed from P(VdF-co-HFP) and liquid electrolyte in the ceramic separator filled void spaces between the nail and electrodes to rapidly recover cell voltage during nail penetration, as shown in Fig 8(b). These results illustrate that the use of a ceramic separator can greatly enhance battery safety while maintaining cycling performance superior to lithium-ion batteries employing the porous polyolefin separator.

4. Conclusions

Ceramic separators based on LLZO were prepared in the form of flexible thin films, and their thermal and electrochemical properties were investigated. The ceramic separators exhibited excellent thermal stability and high ionic conductivity due to the presence of Li^+ ion-conductive LLZO particles. The ceramic separator formed on the negative electrode showed good interfacial adhesion between separator and electrode, resulting in low interfacial resistance and good cycling stability. The lithium-ion batteries assembled with the ceramic separator exhibited superior cycling performance and improved safety when compared to those of a lithium-ion battery employing a conventional PP separator. The ceramic separators in this study are promising for use in rechargeable lithium-ion batteries in emerging applications that require good cycling stability and enhanced safety, such as electric vehicles and energy storage systems.

Acknowledgments

The authors would like to thank Samsung SDI for providing financial support as well as cell fabrication facilities.

References

[1] J.M. Tarascon, M. Armand, Nature 414 (2001) 359–367.
[2] M. Armand, J.M. Tarascon, Nature 451 (2008) 652–657.
[3] P.G. Bruce, B. Scrosati, J.M. Tarascon, Angew. Chem. Int. Ed. 47 (2008) 2930–2946.
[4] J. Hassoun, S. Panero, P. Reale, B. Scrosati, Adv. Mater. 21 (2009) 4807–4810.
[5] V. Etacheri, R. Marom, R. Elazari, G. Salitra, D. Aurbach, Energy Environ. Sci. 4

(2011) 3243–3262.
[6] R. Marom, S.F. Amalraj, N. Leifer, D. Jacob, D. Aurbach, J. Mater. Chem. 21 (2011) 9938–9954.
[7] J.B. Goodenough, K.S. Park, J. Am. Chem. Soc. 135 (2013) 1167–1176.
[8] J.Y. Song, Y.Y. Wang, C.C. Wan, J. Power Sources 77 (1999) 183–197.
[9] M. Armand, F. Endres, D.R. MacFarlane, H. Ohno, B. Scrosati, Nat. Mater. 8 (2009) 621–629.
[10] J.W. Fergus, J. Power Sources 195 (2010) 4554–4569.
[11] J.B. Goodenough, Y. Kim, Chem. Mater. 22 (2010) 587–603.
[12] E. Quartarone, P. Mustarelli, Chem. Soc. Rev. 40 (2011) 2525–2540.
[13] Y.S. Lee, J.H. Lee, J.A. Choi, W.Y. Yoon, D.W. Kim, Adv. Funct. Mater. 23 (2013) 1019–1027.
[14] M. Nagao, H. Kitaura, A. Hayashi, M. Tatsumisago, J. Electrochem. Soc. 160 (2013) A819–A823.
[15] V. Thangadurai, W. Weppner, Adv. Funct. Mater. 15 (2005) 107–112.
[16] R. Murugan, V. Thangadurai, W. Weppner, Angew. Chem. Int. Ed. 46 (2007) 7778–7781.
[17] H. Buschmann, J. Dölle, S. Berendts, A. Kuhn, P. Bottke, M. Wilkening, P. Heitjans, A. Senyshyn, H. Ehrenberg, A. Lotnyk, V. Duppel, L. Kienle, J. Janek, Phys. Chem. Chem. Phys. 13 (2011) 19378–19392.
[18] R. Jalem, Y. Yamamoto, H. Shiiba, M. Nakayama, H. Munakata, T. Kasuga, K. Kanamura, Chem. Mater. 25 (2013) 425–430.
[19] V. Thangadurai, S. Narayanan, D. Pinzaru, Chem. Soc. Rev. 43 (2014) 4714–4727.
[20] R. Djenadic, M. Botros, C. Benel, O. Clemens, S. Indris, A. Choudhary, T. Bergfeldt, H. Hahn, Solid State Ionics 263 (2014) 49–56.
[21] N.M. Asl, J. Keith, C. Lim, L. Zhu, Y. Kim, Electrochim. Acta 79 (2012) 8–16.
[22] T. Inada, K. Takada, A. Kajiyama, M. Kouguchi, H. Sasaki, S. Kondo, M. Watanabe, M. Murayama, R. Kanno, Solid State Ionics 158 (2003) 275–280.
[23] K.M. Nairn, A.S. Best, P.J. Newman, D.R. MacFarlane, M. Forsyth, Solid State Ionics 121 (1999) 115–119.
[24] C. Wang, X.W. Zhang, A.J. Appleby, J. Electrochem. Soc. 152 (2005) A205–A209.
[25] Y. Inda, T. Katoh, M. Baba, J. Power Sources 174 (2007) 741–744.
[26] Y.C. Jung, S.M. Lee, J.H. Choi, S.S. Jang, D.W. Kim, J. Electrochem. Soc. 162 (2015) A704–A710.
[27] C.G. Wu, M.I. Lu, H.J. Chuang, Polymer 46 (2005) 5929–5938.
[28] T. Ma, Z. Cui, Y. Wu, S. Qin, H. Wang, F. Yan, N. Han, J. Li, J. Membr. Sci. 444 (2013) 213–222.
[29] J.R. Kim, S.W. Choi, S.M. Jo, W.S. Lee, B.C. Kim, J. Electrochem. Soc. 152 (2005) A295–A300.
[30] X. Li, G. Cheruvally, J.K. Kim, J.W. Choi, J.H. Ahn, K.W. Kim, H.J. Ahn, J. Power Sources 167 (2007) 491–498.
[31] M. Majima, T. Tada, S. Ujiie, E. Yagasaki, S. Inazawa, K. Miyazaki, J. Power Sources 81–82 (1999) 877–881.
[32] J. Chojnacka, J.L. Acosta, E. Morales, J. Power Sources 97–98 (2001) 819–821.
[33] S.S. Zhang, J. Power Sources 164 (2007) 351–364.
[34] P. Arora, Z. Zhang, Chem. Rev. 104 (2004) 4419–4462.
[35] D. Djian, F. Alloin, S. Martinet, H. Lignier, J.Y. Sanchez, J. Power Sources 172 (2007) 416–421.
[36] Y. Bai, X. Wang, X. Zhang, H. Shu, X. Yang, B. Hu, Q. Wei, H. Wu, Y. Song, Electrochim. Acta 109 (2013) 355–364.
[37] T. Liu, A. Garsuch, F. Chesneau, B.L. Lucht, J. Power Sources 269 (2014) 920–926.
[38] Z. Zhang, D. Fouchard, J.R. Rea, J. Power Sources 70 (1998) 16–20.
[39] J.S. Gnanaraj, E. Zinigrad, L. Asraf, H.E. Gottlieb, M. Sprecher, D. Aurbach, M. Schmidt, J. Power Sources 119–121 (2003) 794–798.
[40] E. Zinigrad, L. Larush-Asraf, J.S. Gnanaraj, H.E. Gottlieb, M. Sprecher, D. Aurbach, J. Power Sources 46 (2005) 176–179.